Case Studies in Construction Materials 22 (2025) e04560

Contents lists available at ScienceDirect

Case Studies in Construction Materials

journal homepage: www.elsevier.com/locate/cscm

Topological effects on the concrete transportation inhibitors: Nano-mechanisms and design principles

Chengbo Liu [a], Yihan Wang [a], Qing Liu [a], Pan Wang [a], Yue Zhang [a], Xinpeng Wang [a], Dongshuai Hou [a], Fengxia Xu [c], Muhan Wang [a,b,*]

[a] Department of Civil Engineering, Qingdao University of Technology, Qingdao 266033, China
[b] Department of Mechanical, Aerospace and Civil Engineering, Brunel University London, Uxbridge, Middlesex UB8 3PH, United Kingdom
[c] College of Biological and Environmental Engineering, Tianjin Vocational Institute, Tianjin 300410, China

ARTICLE INFO

Keywords:
Reinforcement Concrete
Durability
Transportation Inhibitors
Nanoscale
Molecular Design

ABSTRACT

The durability of reinforcement concrete is greatly threatened by the chloride ions (Cl^-) in marine environments, which is attributed to the good permeability of concrete pores where the fluids with Cl^- can easily transport in. Recent studies have been focusing on designing admixtures that can significantly inhibit the transportation of fluids in concrete, but their mechanism of inhibition and designated principle need to be further clarified. Herein, the surfactant-like concrete transportation inhibitors (CTI) with different molecular topologies were investigated to reveal the inhibition mechanism and structural effectiveness by employing molecular dynamics simulations. The increase in nanoscale interfacial tension (IFT) inside the concrete pores is considered to be the origin of transport inhibition. The topological effects of inhibitors on the IFT are also revealed as follows: DTA > DIA > SUA > STA > DBA in which the bola-type structures are recognized as the most competitive ones. Further studies of the nanoscale characteristics from free energy and bonding aspects indicate that the stronger adsorption and stable tails of bola-type structures ensure the best barrier between C-S-H and water, and thus facilitate the highest IFT. Detailed information on the adsorption structures, phase distribution and kinetics properties were also calculated to support this conclusion. This work not only supplies a positive method that can effectively evaluate the properties of CTI in the nanoscale but also can be considered as the beginning of developing concrete admixtures from the molecular design.

1. Introduction

Durability [1,2] poses the paramount issue in the marine infrastructure [3,4] of reinforcement concretes [5] which service life is even halved comparing general environments. Poor durability not only results in structural damage and failure [6], endangering the safe utilization of buildings [7] but also escalates maintenance and reconstruction costs [8] during usage [9]. The primary threat in the marine environment comes from the rich chloride ions (Cl^-) [10–12], which transports to the surface of steel [13], damages the passivation film [14], thereby inducing the corrosion and the subsequent concrete cracking [15]. The transportation of seawater [11,16] is regarded as the motive force in this process. In other words, we can expect to avoid all the negative effects mentioned above if we can effectively inhibit transportation in the concrete pores. Therefore, many researchers have been focusing on developing methods of

* Corresponding author at: Department of Civil Engineering, Qingdao University of Technology, Qingdao 266033, China.
E-mail address: wangmuhan@qut.edu.cn (M. Wang).

https://doi.org/10.1016/j.cscm.2025.e04560
Received 6 January 2025; Received in revised form 28 February 2025; Accepted 18 March 2025
Available online 20 March 2025

transportation inhibition in concrete [17–22].

The current methods of transportation inhibition of Cl^- [22]primarily involve the porosity reduction, ion solidification and electrochemical inhibition et al. Physically, the lower the porosity [23] is, the harder transportation will be, thus when decreasing the water-cement ratio and enhancing concrete compactness can effectively lower the porosity of concrete. Chen et al. [24] investigated the effects of the water-cement (w/c) ratio on the pore structure of cement mortar, which found that the pore structure will become finer and the transportation efficiency will be reduced double when the w/c ratio is reduced by 0.2. However, the chloride ion transportation after the porosity reduction is still very high and needs to be further inhibited [25,26]. Therefore, many studies focus on further methods for inhibition. Introducing the supplementary cementitious materials (SCM) [27] with a rich aluminum phase can effectively solidify the Cl^- that penetrating from environment. Zhang et al. [28] state the enrich aluminum phase of Portland cement can adsorbe 21.32 % ions and thus inhibiting their transportation. Meanwhile, electrochemical inhibition is also a worthwhile attempt, which repair effectively eliminates harmful substances like chloride ions from concrete [29], thereby enhancing durability. Söyl-ev et al. [30] initially delved into the electrochemical corrosion process, while Sánchez et al. [31] proposed an enhanced Electrochemical Chloride Extraction (ECE) configuration via anionic inhibitor migration, thereby boosting electrochemical performance and concrete durability. Such profound methods have the concerns of unstable product performance and high cost respectively, which are also what the field has been committed to solving.

An alternative strategy is employed here, which directly introduces admixtures that can prevent the invasion of fluids with process simplicity and cost-effectiveness.

Improving the transport resistance of concrete by directly adding admixtures has always been the focus of attention. The history of concrete transportation inhibitors traces back to the early 20th century [32] when the challenges of concrete durability, particularly in aggressive environments, became increasingly apparent. Actually, one of the early uses of superplasticizers [33] is to improve the durability of concrete. Until 2004, Knapen et al. [34] suggested a kind of hydrophobic small molecules that can inhibit the transportation of fluids but there are problems with its long-term effectiveness. Zhou et al. [35] proposed that admixtures can inhibit the transportation of ions and that adding some small organic molecules can reduce the ion transportation rate by 17.4 %. Wang et al. [36] work indicates that a molecule can effectively inhibit the transport of ions and fluids if it can effectively increase the interfacial tension between cement hydration products (mostly calcium silicate hydrate, C-S-H [37]) and water in the nanoscale pore, which provides a possibility for designing molecular structures at the nanoscale. The main mechanism of this type of molecule is to inhibit the transport of fluids in concrete, thus referred to as concrete transportation inhibitors (CTI) in this work.

This study primarily focuses on the design of carboxylic acid groups as the main chain for molecular design by using molecular dynamics simulations. It investigates and predicts the performance of CTIs with varying morphological molecular structures and elucidates the interaction mechanisms between these inhibitors and C-S-H. Theoretical calculations are conducted to compare the different molecular structures, and factors influencing variations in the theoretical results are analyzed based on molecular morphology [38–40]. Ultimately, the study identifies the molecular structure with the most robust and stable adsorption performance. The findings indicate that the bola-type CTI exhibits superior competitiveness, effectively increasing interfacial tension by 6 %. The hard structure and two non-competing adsorption functional groups of bola-type CTI are regarded as the origin of the high ability of inhibition of bola-type CTI. This study not only offers a novel approach to the study of corrosion ion inhibitors but also explores the impact of diverse inhibitor molecular structures on inhibition performance, providing valuable insights for the design of more effective environmental inhibitors. These contributions are significant for advancing future research aimed at enhancing the durability of

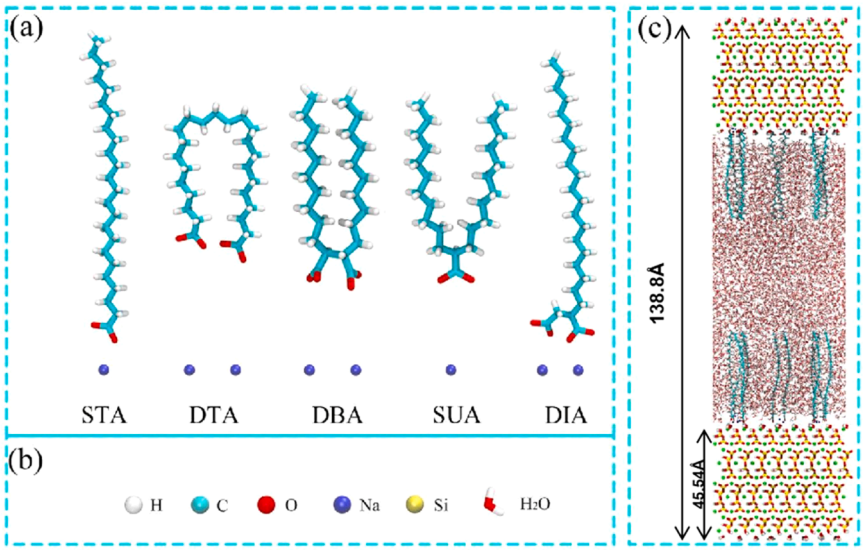

Fig. 1. (a) Molecular structure of CTIs, (b) White, green, red, blue, and yellow balls represent H, C, O, Na, and Si atoms, respectively, and (c) IFT calculation model.

concrete.

2. Computational methods

2.1. Modelling details

To explore the impact of admixtures with varying molecular structures on inhibition performance, we devised five distinct molecular models illustrated in Fig. 1(a). These molecular models are designed by contrasting each other with different numbers of carboxyl groups, and different positions of carboxyl group action. These models were differentiated based on carboxyl group [41] contents and shapes. The newly crafted molecular structures were denoted using the IUPAC nomenclature. From left to right, they are sodium tetracosanoic acid (STA), disodium tetracosanedioic acid (DTA), disodium 2,3-bis(decyl)butanedioic acid (DBA), sodium 2-undecyltridecanoic acid (SUA), and disodium 2-icosylbutanedioic acid (DIA). These designations reflect differences in carboxyl content (STA and DIA vs. DBA and SUA) and structural morphology (DTA, DBA, and DIA). Fig. 1(b) depicts the corresponding atomic species within the design model, while Fig. 1(c) illustrates a conceptual diagram exemplifying CTI. The STA molecule is a widely used, common straight-chain molecule in the market, serving as the foundation for further design expansion. The DTA molecule, a Bola-type molecule, builds upon the STA molecule by adding an adsorption functional group at the opposite end, thereby increasing the number of functional groups and positioning them at both ends of the molecule. In contrast, the DBA molecule features its functional group at the center of the molecular chain, altering the position of action relative to the DTA molecule. Similarly, the SUA molecule has its site of action at the center, differing from the STA molecule, while the DIA molecule has two functional groups acting at the same end, contrasting with the DTA molecule. All these molecules were designed with the premise that they can be synthesized and provide sharp contrasts, facilitating the exploration of the effects and mechanisms of action of CTI molecules.

The molecular modeling process was conducted following the methodologies outlined by Pellenq et al. [42] and Manzano et al. [43] The foundational structure utilized in this study was the C-S-H model with dimensions x = 11.16 Å, y = 7.39 Å, and z = 22.77 Å, as investigated by Murray et al. [44]. To establish the desired C-S-H model with dimensions of x = 44.64 Å, y = 44.34 Å, z = 45.54 Å, and angles a = b = c = 90 degrees, a supercell lattice is employed in the x, y, and z directions, utilizing a 4 × 6 × 2 lattice configuration. The surface non-bridging oxygen is hydroxylated, and selective removal of surface calcium atoms is conducted to preserve overall charge neutrality. The constructed model is contained within a box measuring x = 45.0 Å, y = 45.0 Å, z = 138.8 Å. Subsequently, 10 CTI molecules are situated on both the upper and lower surfaces, and a total of 6600 water molecules are incorporated based on calculations involving water density and molecular weight. This computational model is designed to simulate the initial state of concrete following the addition of an admixture solution within a realistic environment.

2.2. Details of simulation

2.2.1. Force field

The force field serves as the potential function encapsulating interatomic interactions within the simulation. The OPLS (Optimized Potentials for Liquid Simulations) force field stands as a cornerstone in computational chemistry, widely employed for its exceptional accuracy in elucidating MD [45]. Pioneered by W.L. Jorgensen [46] and his team at Ohio State University in the late 1980s and early 1990s, its development represents a seminal achievement in the field. By meticulously optimizing the charge distribution and interatomic interaction parameters, the OPLS force field achieves unparalleled fidelity in describing the intricate properties and behaviors of diverse molecular species. Notably, its superior performance in simulating complex systems has garnered widespread recognition and adoption across various domains of molecular research [47–50]. In this study, we employed the OPLS force field to simulate the interactions among CTI molecules, water molecules, and C-S-H substrates. This approach enabled us to elucidate the intricate mechanisms underlying intermolecular interactions.

2.2.2. Classical molecular dynamics

Molecular dynamics simulations facilitate the investigation of the dynamic behavior of molecular systems, elucidating the intricate interaction processes between atoms and molecules[64–66]. These simulations enable a range of analyses, including interaction analysis and binding free energy calculations, thereby providing powerful tools and methods in the field of molecular design to inform and optimize experimental design.

LAMMPS [51], developed by Sandia National Laboratories, is an open-source software designed for atomic and molecular dynamics simulations. Its primary purpose is to simulate the dynamic behaviors of atomic, molecular, and macromolecular systems. With its versatile capabilities, LAMMPS allows researchers to model a wide range of materials and conditions, making it a valuable tool in various fields such as materials science, chemistry, and biochemistry.

The entire MD process is conducted utilizing the Lammps software, employing the Nose-Hoover thermostat [52] to simulate particle motion within the system by numerically solving the equations of motion derived from Hamiltonian dynamics [53]. This approach maintains a constant temperature throughout the simulation. In the NVT ensemble, the number of particles (N), volume (V), and temperature (T) are kept constant. Widely used in MD simulations because it models system behavior at constant temperature. It is often used to study thermodynamic properties like heat capacity and thermal conductivity. In the NPT ensemble, the number of particles (N), pressure (P), and temperature (T) are kept constant. NPzT then let the pressure in the Z direction be constant and study the behavior of the whole system on the adsorbed surface. Initially, the simulation is performed under the NVT ensemble [54] to optimize the system over a 0.1 ns period, at a constant temperature of 1 K, ensuring the attainment of a fully equilibrated initial state.

Subsequently, simulations are conducted under the NPzT ensemble, with a constant temperature of 298 K, a constant pressure of one atmosphere in the Z direction, and a simulation duration of 1 ns, to observe the system's behavior. Following this, the simulation continues for an additional 5 ns under the same ensemble to achieve system stabilization and acquire a significant dataset. Throughout the process, thermodynamic data such as temperature, pressure, energy, and density are recorded at intervals of every 100 simulation steps to facilitate analysis.

2.3. Umbrella sample

Umbrella Sample (US) [55] is a method used to calculate the potential of mean force (PMF) for a system. It overcomes the challenge of conventional molecular dynamics simulations struggling to adequately sample high energy barrier regions, by restricting the reaction coordinate to a series of windows and enhancing the sampling in the regions of interest. The reaction coordinate is divided into a series of windows, with a harmonic restraint applied in each window to keep the coordinate centered around the window. Independent molecular dynamics simulations are performed in each window, collecting sampling data for the reaction coordinate. The weighted histogram analysis method (WHAM) [56–58] is used to reconstruct the full PMF curve from the windowed sampling data. WHAM can remove the biasing effect of the restraints to recover the true PMF. The PMF curve provides the free energy profile along the reaction coordinate, revealing information like stable conformations and barrier heights. In this study, five CTI molecules were sampled and analyzed according to the US method. Each CTI molecule is divided into 30 panes with a temperature of 298 K and a duration of 3 ns (Fig. 2).

3. Results and discussion

3.1. Performance and structures

3.1.1. Equilibrium structures

The adsorption of CTIs on the surface of C-S-H plays a crucial role and first step in enhancing the stability and durability of C-S-H, thereby mitigating its dissolution and erosion processes. Furthermore, the effective adsorption of these inhibitors can improve the overall performance of concrete and extend its service life. Therefore, investigating the adsorption effects is of paramount importance. After achieving stability in the entire kinetic simulation (as shown in Fig. 3), we selected one of the most representative structures for each molecule to analyze the adsorption behavior post-system stabilization.

All the CTIs are well adsorbed on the C-S-H surface. The STA displayed distinct behavior compared to the other molecules, with some of its molecules positioned further from the C-S-H surface, which influenced overall adsorption effectiveness. This divergence is likely due to STA's weaker adsorption capacity, attributed to its single carboxyl group, longer chain length, and hydrophilic interactions at the hydrophobic terminus, resulting in increased separation. While DTA molecules may separate at one end, the remaining portion adheres to the surface, preserving overall adsorption efficacy. In contrast, the DBA molecule demonstrates superior adsorption, likely due to its structural arrangement, where the carboxyl group is centrally located, effectively dividing the mobile alkane chain into two shorter segments. Additionally, the presence of an extra carboxyl group in DBA, absent in SUA, enhances its adsorption performance. Conversely, both SUA and DIA molecules exhibit instances of detachment from the surface, negatively

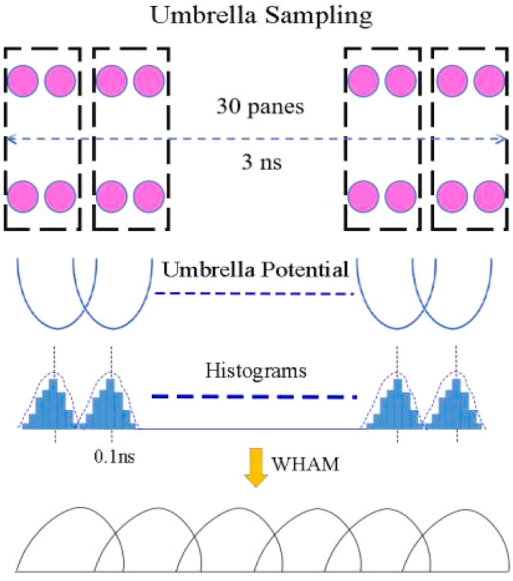

Fig. 2. US diagram: Magenta is the pane sampling, blue is the sampling process, and the black curve is the restructured curve.

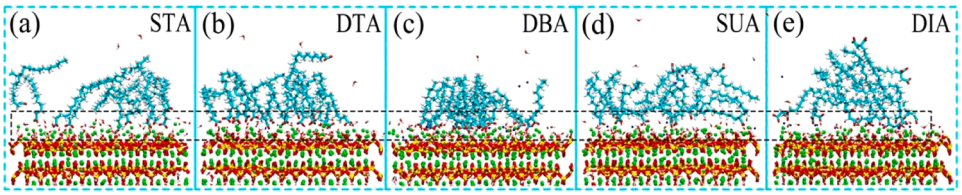

Fig. 3. (a−e)Equilibrium adsorption conformations of five CTI molecules on the C-S-H surface.

affecting overall adsorption efficacy. This phenomenon is presumed to arise from the adsorption of their carboxyl groups with water molecules, coupled with hydrophobic chains generating hydrophilic interactions that promote separation. In summary, each molecule exhibits distinct adsorption characteristics. We will subsequently delve into various aspects of mechanical properties, microstructure, and intermolecular interactions for further analysis.

3.1.2. Relative interfacial tension

Interfacial tension (IFT) characterizes the surface interactions between C-S-H and water in which higher IFT values indicate poorer transportation of the solution [36]. By incorporating CTI, the IFT between the solution and the C-S-H surface can be evaluated. In this study, IFT was calculated for the models with and without CTIs and the differences of IFT are illustrated in Fig. 4.

All CTIs exhibited $\Delta IFT > 0$, indicating an increased IFT and confirming their inhibitory effect on solution erosion. Therefore, the inhibitory ability of the CTIs followed the order: DTA > DIA > SUA > STA > DBA. Overall, the order of ΔIFT appears to correlate with the chain length, where longer chain lengths correspond to larger ΔIFT values. Notably, STA demonstrated a low ΔIFT despite having a sufficient chain length. When comparing DTA and DIA, STA's weak adsorption performance can be attributed to its single carboxyl group, as illustrated in Fig. 3, which shows that STA molecules are positioned further from the adsorbed surface. The results indicate that DTA exhibited the highest ΔIFT, likely due to its two carboxyl groups working synergistically from separate positions, thereby enhancing adsorption effects. In the comparison between DBA and SUA, despite DBA having an additional carboxyl group, its performance remains lower than that of SUA. This phenomenon is presumed to arise from the close proximity of the two carboxyl groups in DBA, leading to competitive interactions during adsorption.

3.1.3. Potential of mean force

To further investigate the adsorption properties of CTIs, the de-adsorption processes were sampled using the umbrella sampling (US) method (Fig. 6), and potential of mean force (PMF) curves were calculated and plotted (Fig. 5). Each PMF curve for the molecules reveals a point of minimum free energy, referred to as the potential well, which corresponds to the most stable adsorption configuration, as it requires the least energy. Conversely, the peaks in the PMF curves represent potential barriers, signifying the energy threshold that the molecule must overcome to transition between different adsorption states or to detach from the adsorbed configuration.

In this case, all of the CTIs have potential barriers and well, indicating that adsorption is present in all of them. The DTA and DBA molecules have the deepest PMF potential wells, indicating the best adsorption for both. While STA has the shallowest potential well and the worst adsorption situation. This is the same as observed in Fig. 3. DTA requires a longer distance from the potential well to the potential barrier and is less likely to reach a desorption situation. Comparing DBA and SUA, SUA, although the number of functional groups has increased, not only has a lower potential barrier but also the distance required from the potential well to the potential

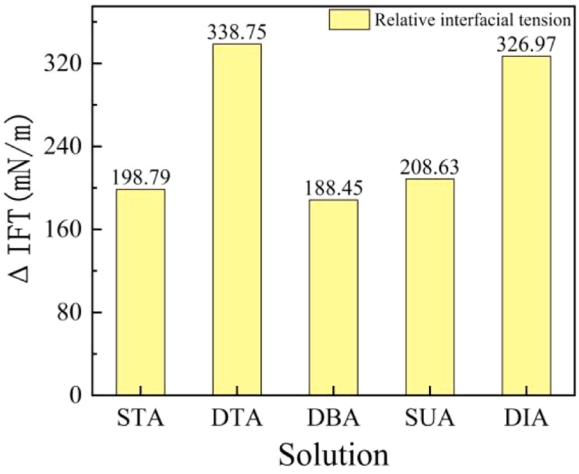

Fig. 4. The ΔIFT of CTIs in aqueous environment, with Δ denoting the difference in IFT from the aqueous environment itself.

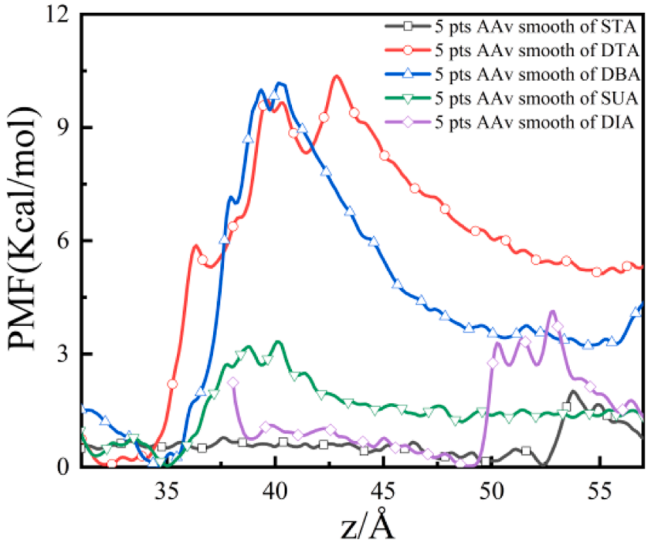

Fig. 5. Potential of mean force curves of five CTI molecules.

barrier has been shortened. This may be because the two functional groups of SUA are close to each other and compete with each other, whereas the two functional groups of DTA work together to produce the adsorption effect. To describe the whole process of sampling more intuitively, the process was plotted with DTA as an example (Fig. 6).

As time progresses, DTA transitions through multiple states. The initial potential well state represents the norm for adsorption, followed by the encounter with two potential barriers, referred to as the Initial Barrier and the Activation Barrier. Upon reaching the Initial Barrier, one of the functional groups is desorbed while the other remains attached, continuing to function as an adsorbent. Once the Activation Barrier is reached, the PMF reaches its peak, leading to the desorption of the second functional group, resulting in the complete detachment of the molecule. Ultimately, diffusion occurs. This observation underscores that the two functional groups of DTA work synergistically to enhance the adsorption effect.

3.2. Micro-structural characticizers

3.2.1. One-dimensional density distribution

To further analyze the structural properties in the nanoscale, the one-dimensional density distribution [59] curves of CTIs are shown in Fig. 7(a-e). The horizontal axis represents the distance of the model in the z-direction, while the vertical axis, g(r), indicates the occurrence frequency of each element. The one-dimensional density distribution comprehensively reflects the constructed model. Notably, the ranges of 48–54 Å and 88–94 Å correspond to the C-S-H adsorption surfaces. It is evident that the peaks for C (Carboxyl) and Ca_{CSH} align on these adsorption surfaces, suggesting that C (Carboxyl) and Ca_{CSH} are primarily responsible for facilitating the adsorption of each molecule.

Numerically, the differences in Ca_{CSH} are more pronounced among CTI molecules with an equivalent number of carboxyl groups, indicating that Ca_{CSH} has a significant influence on adsorption. The sequence of Ca_{CSH} values follows the order DBA > DTA > DIA, which aligns well with the observed adsorption outcomes depicted in Fig. 3.

In terms of peak counts, the highest number of peaks for C (CH_3) is observed in (a), indicating a dispersed distribution of STA's tail chains. This phenomenon is likely due to the softness of its alkane chain, which is susceptible to deformation upon interaction with water molecules, facilitating detachment from the surface and subsequently affecting adsorption efficacy. Similarly, SUA and DIA

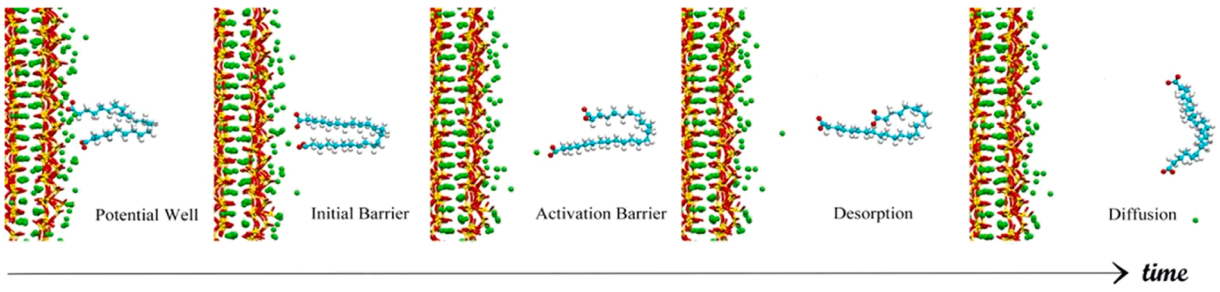

Fig. 6. PMF simulation procedure for a single CTI molecule.

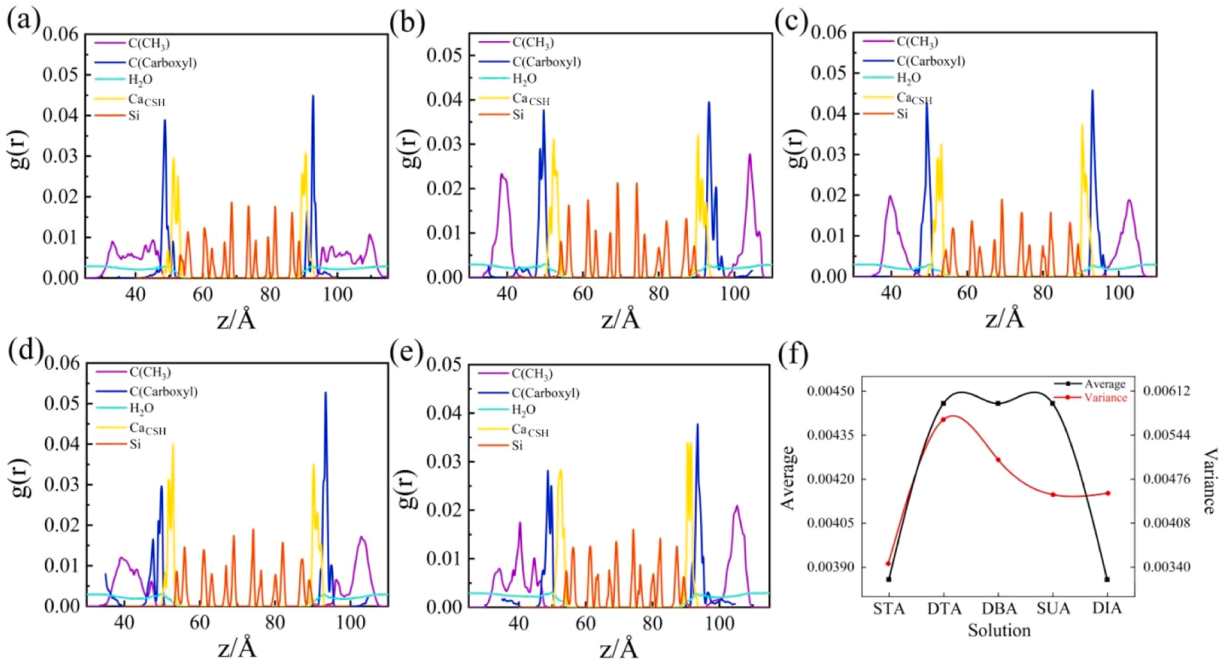

Fig. 7. (a–e) Denote the one-dimensional density distribution curves of STA, DTA, DBA, SUA, and DIA, respectively, and (f) denotes the average and variance of the one-dimensional density distribution of the five molecules $C(CH_3)$. The C (CH_3) denotes the carbon atom at the chain end (in DTA, it refers to the middle carbon atom of the chain). The symbol C (Carboxyl) represents the carbon atom with in the adsorption functional group·H_2O signifies a water molecule, Ca_{CSH} represents a calcium atom located at the surface of the C-S-H, and Si denotes a silicon atom with in the C-S-H.

exhibit a higher peak count, mirroring the observations in STA. Conversely, the sparse occurrence of peaks in (b) and (c) suggests a concentrated distribution of DTA's and DBA's tail links. It is hypothesized that the alkane chains in these molecules are more rigid and less prone to interaction with water molecules, resulting in enhanced adsorption. This observation is consistent with the adsorption trends depicted in Fig. 3.

Fig. 7 **f** illustrates the mean and variance of the one-dimensional density distribution of five $C(CH_3)$ molecules. A higher mean value signifies a greater number of $C(CH_3)$ distributions, while a larger variance indicates a greater degree of dispersion, which in turn suggests a more uniform distribution. Combining these two metrics reveals that the DTA molecules are not only abundant but also uniformly distributed, implying a larger interaction area with water and enhanced inhibition, consistent with the conclusions drawn from the IFT analysis.

3.2.2. Two-dimensional density distribution

Observing adsorption solely in terms of the number of one-dimensional density distributions may lack sufficient detail. In order to assess adsorption more accurately, we calculated two-dimensional density distributions [60] in the X and Y plane directions (Fig. 8).

Overall, the distribution of each molecule in the steady state can be visualised in (a_{1-5}). Use periodic boundary conditions whose alkane chains extending outside the simulation box region are inside the simulation region. The CTI molecular chain depicted in Fig. 8**a** remains within the simulation region, and this plot serves to visualize the chain itself in the top view, facilitating comparative observations with the 2D density distribution. The distribution of (b_{1-5}) is essentially identical to it. Among them, (b2) appears the darkest, suggesting a concentrated distribution of DTA molecules and robust adsorption throughout the simulation. Also from the figure, (b_{1-5}) and (c_{1-5}) complement each other and can form a cohesive whole. The white area in (c2) is more pronounced, followed by (c5), whereas (c1), (c3), and (c4) appear more blurred. The hydrophobicity of DTA is the highest, followed by DIA. And the remaining CTI molecules exhibit inferior hydrophobicity, consistent with the ΔIFT results illustrated in Fig. 4.

When comparing (b_{1-5}) and (d_{1-5}), it becomes apparent that the distribution of DTA alkyl chains and tail chains is largely consistent. This indicates that it is harder overall and the alkane chains are less susceptible to water molecules. The findings are consistent for DBA molecules as well. In contrast, other CTI molecules have large differences in the distribution of alkyl chains and tail links, indicating poor integrity and easy activity of the tail chains, which is consistent with the results speculated in Fig. 7. It was further demonstrated that the adsorption efficacy correlates with the overall softness and hardness of the molecules.

3.2.3. Water order parameter

Different structures of CTI molecules are adsorbed differently on the C-S-H surface, and their hydrophobic chains are longer, which may have an effect on water molecules. The water ordering parameter (WOP) [61] quantifies the degree of order or arrangement of

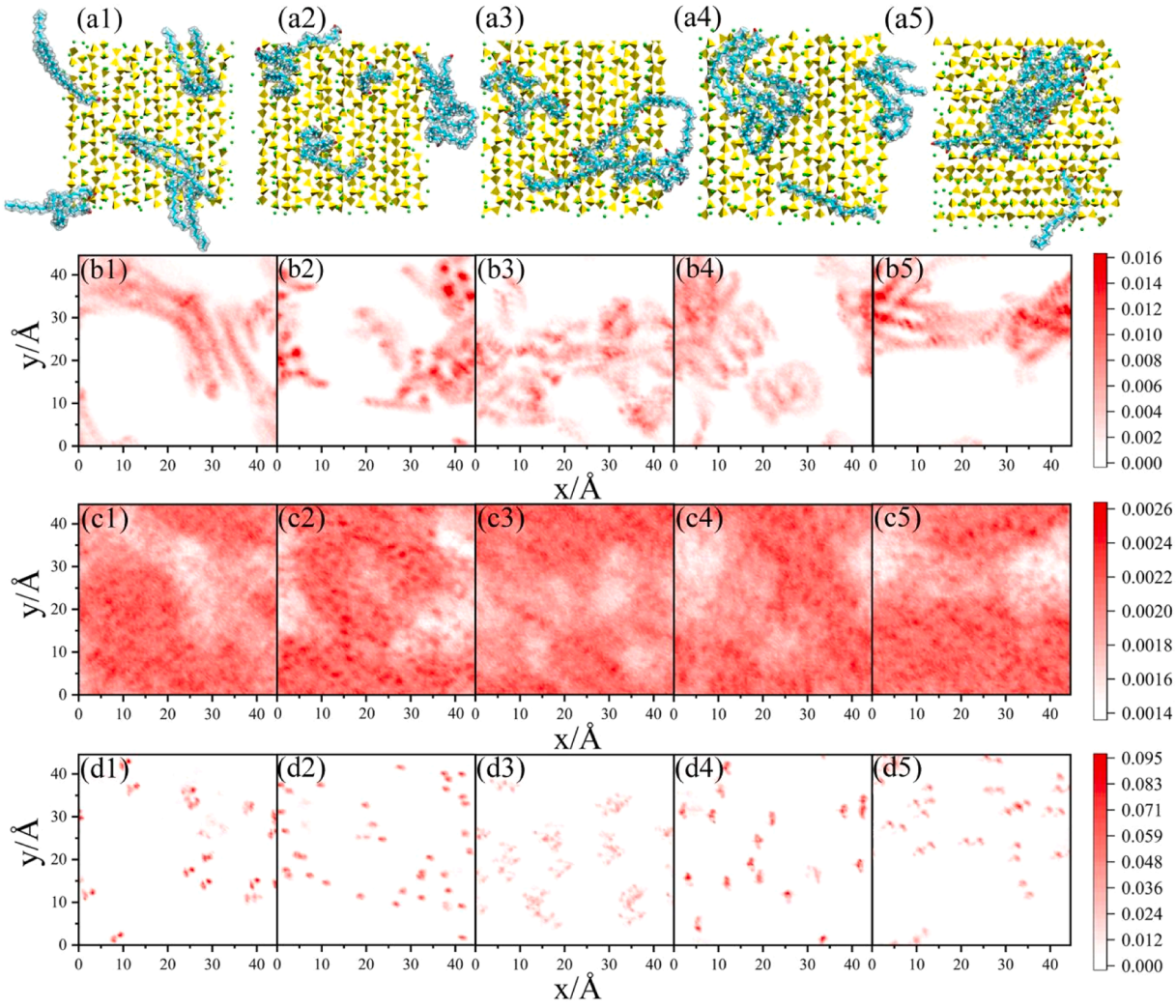

Fig. 8. (a) Depicts the top view of the system post-stabilization, (b-d) illustrate the two-dimensional density distribution of the alkane chain, H_2O, and tail chain, respectively and (1−5) represent the STA, DTA, DBA, SUA, and DIA molecules, respectively.

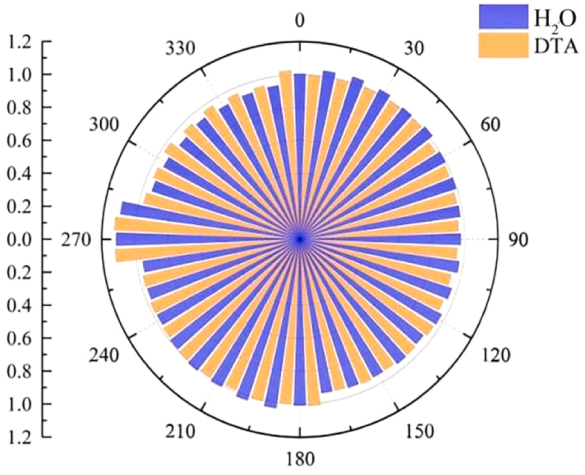

Fig. 9. Dipole direction distribution of water molecules in DTA solution environments.

water molecules. Higher values indicate greater orderliness, while lower values signify less orderliness. Calculating the WOP enables a quantitative assessment of its impact on water molecules. Fig. 9 illustrates WOP calculations employing the DTA molecule as a representative example. Overall, the water exhibits a high degree of orderliness, suggesting that DTA has minimal impact on the arrangement of water molecules. The peaks in the graph correspond to water-induced adsorption effects, with similar outcomes observed for the other CTI molecules.

3.3. Interaction mechanism

RDF describes the spatial distribution of particles, offering structural information about materials. TCF analyzes the dynamic behavior by correlating physical quantities over time, useful for studying diffusion, vibrations, or reaction kinetics. BTE tracks the formation and breaking of bonds over time, providing dynamic insights into chemical reactions or aggregation processes. These methods collectively enhance understanding of molecular interactions and dynamics in simulations.

To delve deeper into the interaction mechanisms among molecules, we performed radial distribution function (RDF) [62] calculations of the C-S-H surface Ca (Ca_{CSH}) and Na with the head group O (O_{CTI}) of the CTI molecule, and Na with O ($O_{W\text{-}CTI}$) in the water of each solution, respectively (Fig. 10). Fig. 10 clearly indicates that Ca_{CSH} and O_{CMI} play significant roles in adsorption. In Fig. 10(a), DTA shows the highest peak, signifying the best adsorption effect, which aligns with the density distribution results. Although DIA has one additional functional group compared to STA, its peak is much lower, suggesting a competitive relationship between the two similar functional groups. Fig. 10(b) reveals that STA has the highest peak, indicating that sodium (Na) binds most effectively to its functional group, which adversely affects its interaction with C-S-H and results in the weakest adsorption. In Fig. 10(c), DIA exhibits the highest perturbation of Na to water, contributing to its elevated IFT. Conversely, DTA shows the lowest peak, suggesting that its higher IFT is not primarily due to Na perturbation but rather to its hydrophobic chain, positioning DTA as the most effective molecule.

Similar conclusions can be drawn from the time correlation function (TCF) [63] and bonding time evolution (BTE) [64] analyses, which serves as a powerful tool for examining time-dependent data, characterizing bond strength and stability.

Figs. 11 and 12 present TCF and BTE analyses. The TCF shows that O_{DTA} exhibits the smoothest bond to Ca_{CSH}, indicating that the adsorption bond is the most stable. The overall line for O_{DTA} reaches the highest value, reflecting both the highest bond energy and the best adsorption performance. In contrast, STA shows a nearly continuous decline, suggesting that this bond is the most unstable and that its energy decreases rapidly over time. Notably, the BTEs of O_{DTA} and Ca_{CSH} demonstrate minimal fluctuations near a value of 1.0, indicating that the chemical bond remains relatively constant over time. This further reinforces the conclusion that DTA possesses the most stable adsorption. DBA also exhibits low fluctuations, which aligns with the observations noted in the adsorption plots.

The root mean square displacement (RMSD) quantifies the average deviation of a molecule from its initial or average structure at a given time, providing insight into the stability and degree of variation of the molecular structure during simulation. A low and stable RMSD value indicates that the molecular structure remains relatively stable, maintaining its initial or average conformation. This typically suggests that the molecule exhibits better stability under the simulated conditions. Conversely, high and fluctuating RMSD values may indicate structural instability, with the molecule undergoing significant conformational changes. This information is crucial for understanding the mechanism of action and stability of the molecule.

For evaluating the stability of adsorption, the RMSD [65,66] of molecular conformations in the last 1000 frames can be calculated to describe the changes and stability (Fig. 13).

For the DTA molecule, the RMSD value is relatively small and exhibits minimal variation, indicating that the molecule maintained a stable conformation over the last 1000 frames. This stability suggests that the structural form of the DTA molecule is robust. In contrast, the STA molecule, despite the system reaching a stable state during the last 1000 frames, shows a significant range of variation in its RMSD value. This indicates that the structural form of the STA molecule is relatively unstable, with its conformation continuously fluctuating even in the stable state. Therefore, RMSD analysis reveals that the DTA molecule exhibits greater structural stability compared to the less stable STA molecule.

4. Conclusion

In conclusion, this study elucidates the inhibition mechanisms of surfactant-like concrete transportation inhibitors (CTI) in reinforcing concrete against chloride ion transportation. Through molecular dynamics simulations, the research demonstrates that the bola-type structures significantly enhance nanoscale interfacial tension (IFT), thereby serving as effective barriers against fluid transport. The findings emphasize the critical role of molecular topology in optimizing the structural effectiveness of CTIs, providing a foundation for future molecular design of concrete admixtures. The details are following:

(1) All of the surfactant-like CTIs can increase the IFT between C-S-H and water, and the topologies can significantly affect the performance of CTIs, of which the IFT rank is DTA > DIA > SUA > STA > DBA. The molecular dynamics methods can supply a method to evaluate the IFT in the nanoscale, which avoids the Difficulty of the experimental measurement.

(2) All of the CTIs adsorb on C-S-H through the carboxylates on their headgroups. Generally, the more carboxylates are, the stronger adsorption will be. But the two carboxylates shouldn't be topological approaching that can attribute a competitive effect that is not conducive to adsorption. Bola-type molecules of CTIs show minimal effects between carboxyl groups.

(3) The bola-type CTI structure provides the most effective barrier between C-S-H and water, thereby enhancing the IFT. This phenomenon is primarily due to the harder conformation of the tails for this type of molecule. Also, the bola-type molecule has the best resistance to desorption because it can take advantage of the detachment of one functional group while keeping the adsorption of another functional group stable.

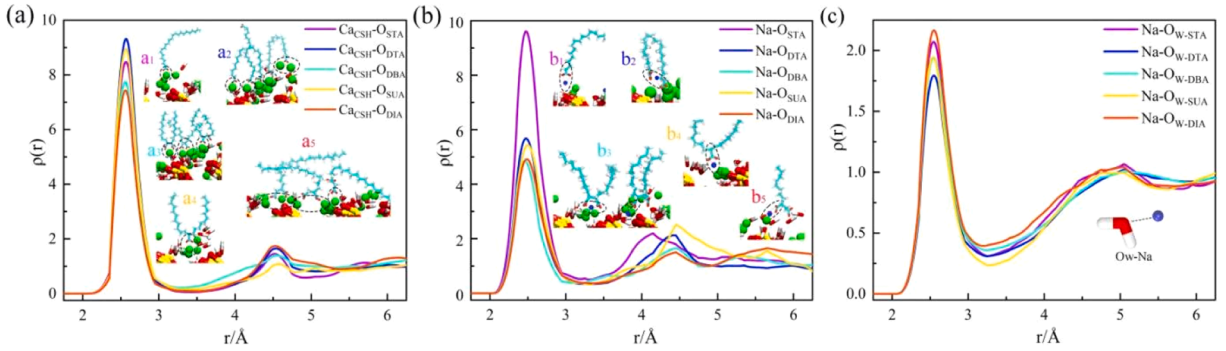

Fig. 10. (a-c) represent the RDF of Ca_{CSH} with O_{CTI}, Na with O_{CTI}, and Na with $O_{W\text{-}CTI}$, respectively.

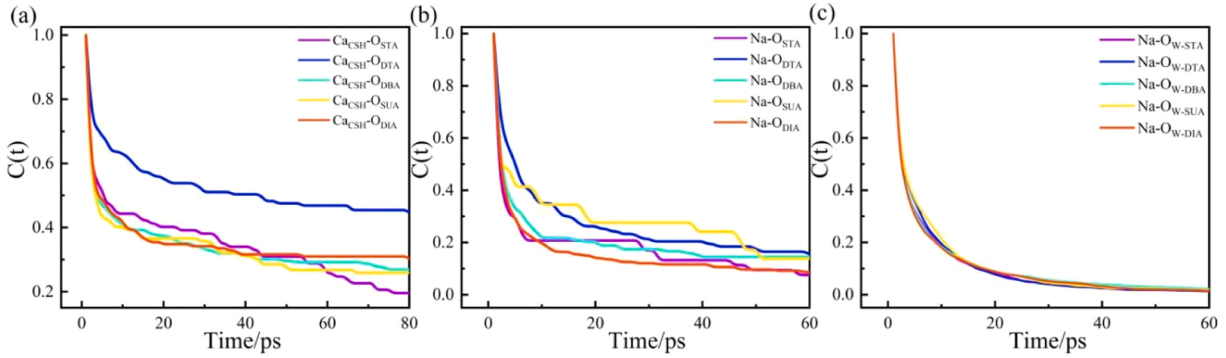

Fig. 11. (a-c) represent the TCF of Ca_{CSH} with O_{CTI}, Na with O_{CTI}, and Na with $O_{W\text{-}CTI}$, respectively.

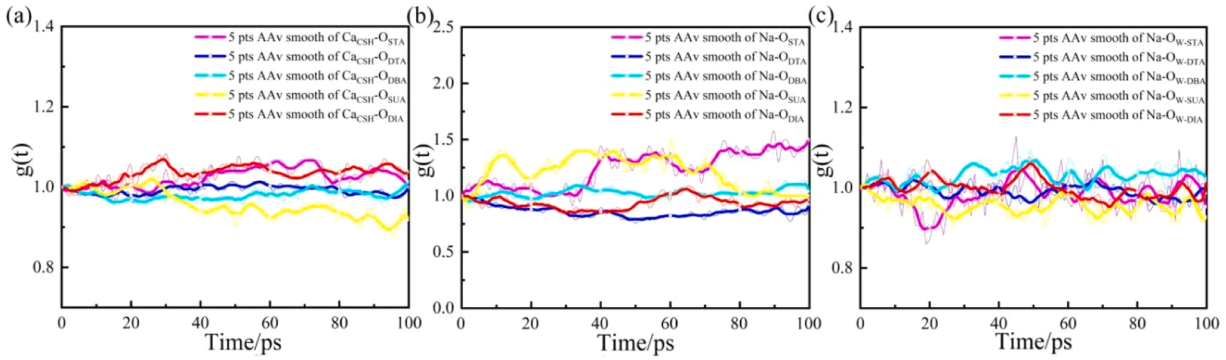

Fig. 12. (a-c) represent the BTE of Ca_{CSH} with O_{CTI}, Na with O_{CTI}, and Na with $O_{W\text{-}CTI}$, respectively.

This investigation leads to a possible new direction for understanding the mechanism of CTIs in concrete systems. In the future, it will be desirable to synthesize these molecules and move towards more complex systems. These works provide an excellent approach for observing and revealing the microscopic structural properties of CTIs. The revealing mechanism can be further used to evaluate the performance of the different concrete systems in an intuitive and theoretical approach.

CRediT authorship contribution statement

Liu Chengbo: Writing – original draft, Software, Investigation, Data curation. **Wang Yihan:** Data curation. **Liu Qing:** Writing – review & editing. **Hou Dongshuai:** Writing – review & editing. **Wang Muhan:** Writing – review & editing, Supervision, Methodology, Conceptualization. **Wang Pan:** Writing – review & editing. **Zhang Yue:** Writing – review & editing. **Wang Xinpeng:** Writing – review & editing. **Xu Fengxia:** Writing – review & editing.

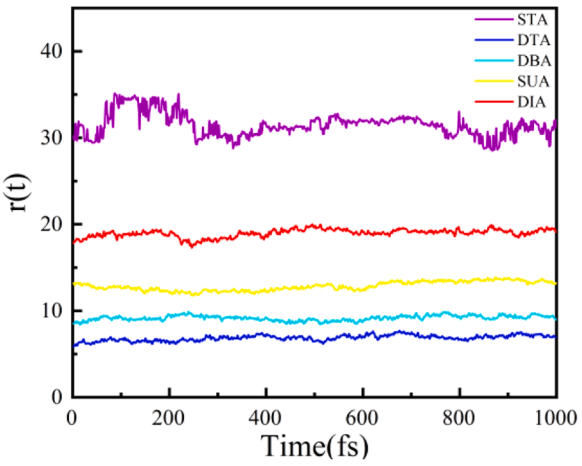

Fig. 13. Root mean square displacement analysis of CTI molecules.

Declaration of Competing Interest

No conflict of interest is declared.

Acknowledgment

M. W. and D. H. financial support from the National Key Research and Development Project 2022YFE0133800, National Natural Science Foundation of China under Grant U2006224, 52308263, 51978352, 52178221, Natural Science Foundation of Shandong Province under Grant ZR2020JQ25, ZR2022YQ55, Shandong Provincial Education Department under Grant 2023KJ320, 2019KJG010, Qingdao Research Program 16–5–1–96-jch, 111 Project TMduracon20220022, Taishan Scholars of Shandong Province under Grant 201812090, Royal Society under Grant NIF\R1\242498, are gratefully acknowledged.

Data availability

The data that has been used is confidential.

References

[1] K.L. Scrivener, R.J. Kirkpatrick, Innovation in use and research on cementitious material, Cem. Concr. Res. 38 (2) (2008) 128–136.
[2] S.W. Tang, Y. Yao, C. Andrade, Z.J. Li, Recent durability studies on concrete structure, Cem. Concr. Res. 78 (2015) 143–154.
[3] Y. Yi, D. Zhu, S. Guo, Z. Zhang, C. Shi, A review on the deterioration and approaches to enhance the durability of concrete in the marine environment, Cem. Concr. Compos 113 (2020) 103695.
[4] F. Qu, W. Li, W. Dong, V.W.Y. Tam, T. Yu, Durability deterioration of concrete under marine environment from material to structure: a critical review, J. Build. Eng. 35 (2021) 102074.
[5] Z. Li, X. Zhou, H. Ma, D. Hou, Advanced Concrete Technology, John Wiley \& Sons, 2022.
[6] F. Biondini, D.M. Frangopol, Time-Variant Redundancy and Failure Times of Deteriorating Concrete Structures Considering Multiple Limit States. In *Structures and Infrastructure Systems*, Routledge, 2019, pp. 418–430.
[7] J.R. Krentowski, Assessment of destructive impact of different factors on concrete structures durability, Mater. (Basel) 15 (1) (2021) 225.
[8] J.L. Provis, Alkali-Activated Materials, Cem. Concr. Res. 114 (2018) 40–48.
[9] M.G. Alexander, M. Santhanam, Y. Ballim, Durability design and specification for concrete structures——the way forward, Int. J. Adv. Eng. Sci. Appl. Math. 2 (2010) 95–105.
[10] B. Da, H. Yu, H. Ma, Y. Tan, R. Mi, X. Dou, Chloride diffusion study of coral concrete in a marine environment, Constr. Build. Mater. 123 (2016) 47–58.
[11] J. Zuquan, Z. Xia, Z. Tiejun, L. Jianqing, Chloride ions transportation behavior and binding capacity of concrete exposed to different marine corrosion zones, Constr. Build. Mater. 177 (2018) 170–183.
[12] H.E.-D.H. Seleem, A.M. Rashad, B.A. El-Sabbagh, Durability and strength evaluation of high-performance concrete in marine structures, Constr. Build. Mater. 24 (6) (2010) 878–884.
[13] V. Kumar, Protection of steel reinforcement for concrete-a review, Corros. Rev. 16 (4) (1998) 317–358.
[14] Y. Wang, S. Nanukuttan, Y. Bai, P.A.M. Basheer, Influence of combined carbonation and chloride ingress regimes on rate of ingress and redistribution of chlorides in concretes, Constr. Build. Mater. 140 (2017) 173–183.
[15] S. Mosallanejad, I. Oluwoye, M. Altarawneh, J. Gore, B.Z. Dlugogorski, Interfacial and bulk properties of concentrated solutions of ammonium nitrate, Phys. Chem. Chem. Phys. 22 (47) (2020) 27698–27712, https://doi.org/10.1039/d0cp04874g.
[16] O.E. Gjørv, Ø. Vennesland, Diffusion of chloride ions from seawater into concrete, Cem. Concr. Res. 9 (2) (1979) 229–238.
[17] Y. Bai, P.A.M. Basheer, Influence of furnace bottom ash on properties of concrete, Proc. Inst. Civ. Eng. Build. 156 (1) (2003) 85–92.
[18] H. Saricimen, M. Mohammad, A. Quddus, M. Shameem, M.S. Barry, Effectiveness of concrete inhibitors in retarding rebar corrosion, Cem. Concr. Compos 24 (1) (2002) 89–100.
[19] N.R. Buenfeld, G.K. Glass, A.M. Hassanein, J.-Z. Zhang, Chloride transport in concrete subjected to electric field, J. Mater. Civ. Eng. 10 (4) (1998) 220–228.
[20] Y. Liu, X. Shi, Electrochemical chloride extraction and electrochemical injection of corrosion inhibitor in concrete: state of the knowledge, Corros. Rev. 27 (1–2) (2009) 53–82.

[21] V. Saraswathy, H.-W. Song, Improving the durability of concrete by using inhibitors, Build. Environ. 42 (1) (2007) 464–472.
[22] B. Dong, H. Diao, H. Ren, S. Hong, Y. Wang, G. Fang, Y. Zhang, Chloride-ion-triggered microcapsule for self-suppression of capillary suction in cement paste, Cem. Concr. Compos 141 (2023) 105144.
[23] K.L. Scrivener, A.K. Crumbie, P. Laugesen, The interfacial transition zone (ITZ) between cement paste and aggregate in concrete, Interface Sci. 12 (2004) 411–421.
[24] X. Chen, S. Wu, Influence of water-to-cement ratio and curing period on pore structure of cement mortar, Constr. Build. Mater. 38 (2013) 804–812.
[25] G. Dai, Q. Wu, K. Lu, S. Ma, W. Wang, H. Zhou, C. Cai, Z. Han, J. Chen, Study of chloride ion diffusion in coral aggregate seawater concrete with different water–cement ratios under load, Mater. (Basel) 16 (2) (2023) 869.
[26] Y. Li, G. Zhang, J. Yang, Y. Ding, Q. Ding, Y. Wang, Chloride ion transport properties in lightweight ultra-high-performance concrete with different lightweight aggregate particle sizes, Mater. (Basel) 15 (19) (2022) 6626.
[27] B. Lothenbach, K. Scrivener, R.D. Hooton, Supplementary cementitious materials, Cem. Concr. Res. 41 (12) (2011) 1244–1256.
[28] G. Zhang, M. Li, Z. Zhu, Effect of aluminium substitution on physical adsorption of chloride and sulphate ions in cement-based materials, Materials 16 (17) (2023) 6029.
[29] W. Fan, J. Mao, W. Jin, J. Zhang, Q. Li, F. Yuan, Repair effect of cracked reinforced concrete based on electrochemical rehabilitation technology, J. Build. Eng. 61 (2022) 105211.
[30] T.A. Söylev, M.G. Richardson, Corrosion inhibitors for steel in concrete: state-of-the-art report, Constr. Build. Mater. 22 (4) (2008) 609–622.
[31] M. Sánchez, M.C. Alonso, Electrochemical chloride removal in reinforced concrete structures: improvement of effectiveness by simultaneous migration of calcium nitrite, Constr. Build. Mater. 25 (2) (2011) 873–878.
[32] N.R. Buenfeld, J.B. Newman, The permeability of concrete in a marine environment, Mag. Concr. Res. 36 (127) (1984) 67–80.
[33] V.M. Malhotra, Effect of Repeated Dosages of Superplasticizers on Workability, Strength and Durability of Concrete. In *Advances in Concrete Slab Technology*, Elsevier, 1980, pp. 49–57.
[34] E. Knapen, A. Beeldens, D. Van Gemert, F. Van Rickstal, Modification of cement concrete by means of polymers in solution, Proc. 11th Congr. Polym. Concr. (2004) 83–90.
[35] Y. Zhou, J. Cai, R. Chen, D. Hou, J. Xu, K. Lv, Q. Zheng, The Design and evaluation of a smart polymer-based fluids transport inhibitor, J. Clean. Prod. 257 (2020) 120528.
[36] M. Wang, H. Sun, X. Zhou, P. Wang, Z. Li, D. Hou, Surface engineering of migratory corrosion inhibitors: controlling the wettability of calcium silicate hydrate in the nanoscale, Langmuir 39 (48) (2023) 17110–17121, https://doi.org/10.1021/acs.langmuir.3c01953.
[37] K.L. Scrivener, A. Nonat, Hydration of cementitious materials, present and future, Cem. Concr. Res. 41 (7) (2011) 651–665.
[38] M. Wang, K. Zhang, X. Ji, et al., Molecular insight into the fluidity of cement pastes: Nano-boundary lubrication of cementitious materials, Constr. Build. Mater. 316 (2022) 125800.
[39] M. Wang, S. Wu, P. Wang, et al., Nano-deterioration of steel passivation film: chloride attack in material defects, Mater. Struct. 56 (2) (2023) 35.
[40] M. Wang, S. Yu, C. Liu, et al., Design of high chloride-resistant passivation films: From synthesis to the mechanisms of nano-generation, Corros. Sci. 244 (2025) 112656.
[41] Q. Liu, C. Liu, M. Wang, X. Ji, F. Hong, D. Hou, J. Zhang, M. Wang, Advancing understanding of polymer-based superplasticizers for diverse concrete applications: insights from quantum chemistry and nanoscale adsorption behavior, Cem. Concr. Compos 153 (2024) 105690.
[42] R.J.-M. Pellenq, A. Kushima, R. Shahsavari, K.J. Van Vliet, M.J. Buehler, S. Yip, F.-J. Ulm, A realistic molecular model of cement hydrates, Proc. Natl. Acad. Sci. 106 (38) (2009) 16102–16107.
[43] H. Manzano, S. Moeini, F. Marinelli, A.C.T. Van Duin, F.-J. Ulm, R.J.-M. Pellenq, Confined water dissociation in microporous defective silicates: mechanism, dipole distribution, and impact on substrate properties, J. Am. Chem. Soc. 134 (4) (2012) 2208–2215.
[44] S.J. Murray, V.J. Subramani, R.P. Selvam, K.D. Hall, Molecular dynamics to understand the mechanical behavior of cement paste, Transp. Res. Rec. 2142 (1) (2010) 75–82.
[45] H. Guo, Q. Tang, P. Wang, M. Wang, Y. Zhang, A. Liu, D. Hou, Exploration of adsorption properties of organic corrosion inhibitors on layered double hydroxide nanosheet: a molecular dynamics simulation study, Appl. Clay Sci. 260 (2024) 107548.
[46] W.L. Jorgensen, J. Tirado-Rives, The OPLS [optimized potentials for liquid simulations] potential functions for proteins, energy minimizations for crystals of cyclic peptides and crambin, J. Am. Chem. Soc. 110 (6) (1988) 1657–1666.
[47] W.L. Jorgensen, E.R. Laird, T.B. Nguyen, J. Tirado-Rives, Monte Carlo simulations of pure liquid substituted benzenes with OPLS potential functions, J. Comput. Chem. 14 (2) (1993) 206–215.
[48] J.P. Ulmschneider, M.B. Ulmschneider, United atom lipid parameters for combination with the optimized potentials for liquid simulations all-atom force field, J. Chem. Theory Comput. 5 (7) (2009) 1803–1813.
[49] J. Gao, Toward a molecular orbital derived empirical potential for liquid simulations, J. Phys. Chem. B 101 (4) (1997) 657–663.
[50] I. Yungerman, I. Starodumov, A. Fulati, K. Uto, M. Ebara, Y. Moskovitz, Full-atomistic optimized potentials for liquid simulations and polymer consistent force field models for biocompatible shape-memory poly (E-Caprolactone), J. Phys. Chem. B 126 (21) (2022) 3961–3972.
[51] A.P. Thompson, H.M. Aktulga, R. Berger, D.S. Bolintineanu, W.M. Brown, P.S. Crozier, In't Veld, P. J.; Kohlmeyer, A.; Moore, S. G.; Nguyen, T. D.; others. LAMMPS-a Flexible simulation tool for particle-based materials modeling at the atomic, meso, and continuum scales, Comput. Phys. Commun. 271 (2022) 108171.
[52] D.J. Evans, B.L. Holian, The nose–hoover thermostat, J. Chem. Phys. 83 (8) (1985) 4069–4074.
[53] P.A.M. Dirac, Generalized hamiltonian dynamics, Can. J. Math. 2 (1950) 129–148.
[54] S. Nosé, A molecular dynamics method for simulations in the canonical ensemble, Mol. Phys. 52 (2) (1984) 255–268.
[55] B. Roux, The calculation of the potential of mean force using computer simulations, Comput. Phys. Commun. 91 (1–3) (1995) 275–282.
[56] M. Souaille, B. Roux, Extension to the weighted histogram analysis method: combining umbrella sampling with free energy calculations, Comput. Phys. Commun. 135 (1) (2001) 40–57.
[57] S. Kumar, J.M. Rosenberg, D. Bouzida, R.H. Swendsen, P.A. Kollman, Multidimensional free-energy calculations using the weighted histogram analysis method, J. Comput. Chem. 16 (11) (1995) 1339–1350.
[58] S. Kumar, J.M. Rosenberg, D. Bouzida, R.H. Swendsen, P.A. Kollman, The weighted histogram analysis method for free-energy calculations on biomolecules. I. The method, J. Comput. Chem. 13 (8) (1992) 1011–1021.
[59] T. Passot, E. Vázquez-Semadeni, Density probability distribution in one-dimensional polytropic gas dynamics, Phys. Rev. E 58 (4) (1998) 4501.
[60] M. Rovere, D.W. Hermann, K. Binder, Block density distribution function analysis of two-dimensional lennard-jones fluids, Europhys. Lett. 6 (7) (1988) 585.
[61] J.R. Errington, P.G. Debenedetti, Relationship between structural order and the anomalies of liquid water, Nature 409 (6818) (2001) 318–321.
[62] A.P. Lyubartsev, A. Laaksonen, Calculation of effective interaction potentials from radial distribution functions: a reverse monte carlo approach, Phys. Rev. E 52 (4) (1995) 3730.
[63] G.D. Harp, B.J. Berne, Time-correlation functions, memory functions, and molecular dynamics, Phys. Rev. A 2 (3) (1970) 975.
[64] S. Toxvaerd, O.J. Heilmann, T. Ingebrigtsen, T.B. Schrøder, J.C. Dyre, Time-reversible molecular dynamics algorithms with bond constraints, J. Chem. Phys. 131 (6) (2009).
[65] K. Sargsyan, C. Grauffel, C. Lim, How molecular size impacts RMSD applications in molecular dynamics simulations, J. Chem. Theory Comput. 13 (4) (2017) 1518–1524.
[66] O. Carugo, How root-mean-square distance (RMSD) values depend on the resolution of protein structures that are compared, J. Appl. Crystallogr 36 (1) (2003) 125–128.